Predictive modelling of rainfall-induced landslide hazard in the Lesser Himalaya of Nepal based on weights-of-ev...

Santosh Dhakal

Geomorphology

Geomorphology xxx (2008) xxx-xxx

Contents lists available at ScienceDirect

Geomorphology

journal homepage: www.elsevier.com/locate/geomorph

Predictive modelling of rainfall-induced landslide hazard in the Lesser Himalaya of Nepal based on weights-of-evidence

Ranjan Kumar Dahal [a,b,*], Shuichi Hasegawa [a], Atsuko Nonomura [a], Minoru Yamanaka [a], Santosh Dhakal [c], Pradeep Paudyal [d]

[a] Department of Safety Systems Construction Engineering, Faculty of Engineering, Kagawa University, 2217-20, Hayashi-cho, Takamatsu City, 761-0396, Japan
[b] Department of Geology, Tri-Chandra Multiple Campus, Tribhuvan University, Ghantaghar, Kathmandu, Nepal
[c] Department of Mines and Geology, Lainchaur, Kathmandu, Nepal
[d] Mountain Risk Engineering Unit, Tribhuvan University, Kirtipur, Kathmandu, Nepal

ARTICLE INFO

Article history:
Received 9 December 2007
Received in revised form 19 May 2008
Accepted 20 May 2008
Available online xxxx

Keywords:
Lesser Himalaya
Nepal
Landslides
Weights-of-evidence
GIS
Landslide hazard mapping

ABSTRACT

Landslide hazard mapping is a fundamental tool for disaster management activities in mountainous terrains. The main purpose of this study is to evaluate the predictive power of weights-of-evidence modelling in landslide hazard assessment in the Lesser Himalaya of Nepal. The modelling was performed within a geographical information system (GIS), to derive a landslide hazard map of the south-western marginal hills of the Kathmandu Valley. Thematic maps representing various factors (e.g., slope, aspect, relief, flow accumulation, distance to drainage, soil depth, engineering soil type, landuse, geology, distance to road and extreme one-day rainfall) that are related to landslide activity were generated, using field data and GIS techniques, at a scale of 1:10,000. Landslide events of the 1970s, 1980s, and 1990s were used to assess the Bayesian probability of landslides in each cell unit with respect to the causative factors. To assess the accuracy of the resulting landslide hazard map, it was correlated with a map of landslides triggered by the 2002 extreme rainfall events. The accuracy of the map was evaluated by various techniques, including the area under the curve, success rate and prediction rate. The resulting landslide hazard value calculated from the old landslide data showed a prediction accuracy of >80%. The analysis suggests that geomorphological and human-related factors play significant roles in determining the probability value, while geological factors play only minor roles. Finally, after the rectification of the landslide hazard values of the new landslides using those of the old landslides, a landslide hazard map with >88% prediction accuracy was prepared. The methodology appears to have extensive applicability to the Lesser Himalaya of Nepal, with the limitation that the model's performance is contingent on the availability of data from past landslides.

1. Introduction

Landslides are among the most damaging natural hazards in the mountainous terrains of the Lesser Himalaya of Nepal. Sites that are particularly at risk for landslides should therefore be identified so as to reduce damage in the region. Landslide hazard assessment has become a vital subject for authorities responsible for infrastructural development and environmental protection. Much research has been carried out to prepare landslide susceptibility and landslide hazard maps. According to Varnes (1984), landslide hazard in a given area can be assessed in terms of probability of occurrence of a potentially damaging landslide event within a specified period. Both intrinsic and extrinsic variables affect landslide hazards (Siddle et al., 1991; Wu and Sidle, 1995; Atkinson and Massari, 1998; Dai et al., 2001; Çevik and Topal, 2003). Intrinsic variables determining hazards include bedrock geology, topography, soil depth, soil type, slope gradient, slope aspect, slope curvature, elevation, engineering properties of the slope material, land use pattern, and drainage patterns. Extrinsic variables include heavy rainfall, earthquakes, and volcanic activities. Although the probability of landslide occurrence depends on both intrinsic and extrinsic variables, the latter possess a temporal distribution which is more difficult to handle in modelling practice. Therefore, for landslide hazard assessment, "landslide susceptibility mapping" is often conducted in which the extrinsic variables are not considered in determining the probability of landslide occurrence (Dai et al., 2001). In this research, a landslide hazard map was prepared by considering the extrinsic variable of rainfall in addition to the intrinsic variables.

There have been numerous studies involving landslide hazard evaluation (Guzetti et al., 1999). Landslide hazard may be assessed through heuristic, deterministic, and statistical approaches (Yin and Yan, 1988; Van Westen and Terlien, 1996; Gökceoglu and Aksoy, 1996;

* Corresponding author. Department of Safety Systems Construction Engineering, Faculty of Engineering, Kagawa University, 2217-20, Hayashi-cho, Takamatsu City, 761-0396, Japan. Tel.: +81 87 864 2140; fax: +81 87 864 2031.
E-mail addresses: ranjan@ranjan.net.np, rkdahal@yahoo.com (R.K. Dahal).
URL: http://www.ranjan.net.np (R.K. Dahal).

0169-555X/$ – see front matter © 2008 Elsevier B.V. All rights reserved.
doi:10.1016/j.geomorph.2008.05.041

Pachauri et al., 1998; Van Westen, 2000; Lee and Min, 2001; Dai et al., 2001; Van Westen et al., 2003; Zêzere et al., 2004; Süzen and Doyuran, 2004; Saha et al., 2005; Dahal et al., 2008; Sharma and Kumar, 2008). A heuristic approach is a direct or semi-direct mapping methodology in which a relationship is established between the occurrence of slope failures and the causative factors. In this approach the opinions of experts are very important in estimating landslide potential from the data for intrinsic variables. Therefore, assigning weight values and ratings to the variables is very subjective, and the results are often not reproducible. Deterministic approaches, in contrast, are based on slope stability analyses, and are only applicable when the ground conditions are relatively homogeneous across the study area and the landslide types are known. The infinite slope stability model has been widely used in the deterministic approaches (Wu and Sidle, 1995; Terlien, 1996; Gökceoglu and Aksoy, 1996), and such models need a high degree of simplification of the intrinsic variables. Statistical approaches, on the other hand, are indirect hazard mapping methodologies that involve statistical determination of the combinations of variables that have led to landslide occurrence in the past. All possible intrinsic variables are entered into a Geographical Information System (GIS) and integrated with a landslide inventory map. Both bivariate and multivariate statistical methods have been used in such approaches (Siddle et al., 1991; Atkinson and Massari, 1998; Van Westen, 2000; Dai et al., 2001; Dahal et al., 2008; Neuhäuser and Terhorst, 2007). Keeping this in mind, this study evaluates the landslide hazard through GIS techniques using weights-of-evidence modelling with respect to a bivariate statistical approach. The study area in the south-western hills of the Kathmandu Valley experienced extensive landslide damage during the heavy monsoon rainfall of 2002, and thus is suitable for the evaluation of rainfall-induced landslide hazard in the Lesser Himalaya of Nepal.

Various models have been applied to landslide susceptibility and hazard mapping in the last 25 years (Guzetti et al., 1999; Chung and Fabbri, 2003; Remondo et al., 2003; Van Westen et al., 2003; Lee, 2004). In many landslide susceptibility and hazard mappings, however, independent validation of statistical models for landslide hazard or susceptibility assessment is lacking. A time-based separation of landslides, i.e., use of older landslides for modelling and new landslides for validation, is the most acceptable method of validation (Van Westen et al., 2003). One of the objectives of the present study is to perform such validation. The other main objectives of this paper are: 1) to employ weights-of-evidence modelling with a bivariate statistical approach to define the physical parameters contributing to the occurrence of landslides in the Lesser Himalaya, and 2) to prepare a landslide hazard map that possesses high prediction and success rates for the study area.

2. The study area

The study area is located in the south-western hills of the Kathmandu Valley, Lesser Himalaya, Nepal (Fig. 1). The Kathmandu Valley is the largest intermontane basin of the Lesser Himalaya (Ganser, 1964), and is surrounded by high-relief mountains such as Shivapuri (2732 m) in the north, Phulchowki (2762 m) in the southeast, and Chandragiri (2543 m) in the southwest. Nepal is divided into five tectonic zones from north to south: the Tibetan–Tethys Himalayan, Higher Himalayan, Lesser Himalayan, Siwalik, and Terai zones (Fig. 2A). Among them, the Lesser Himalayan and Siwalik

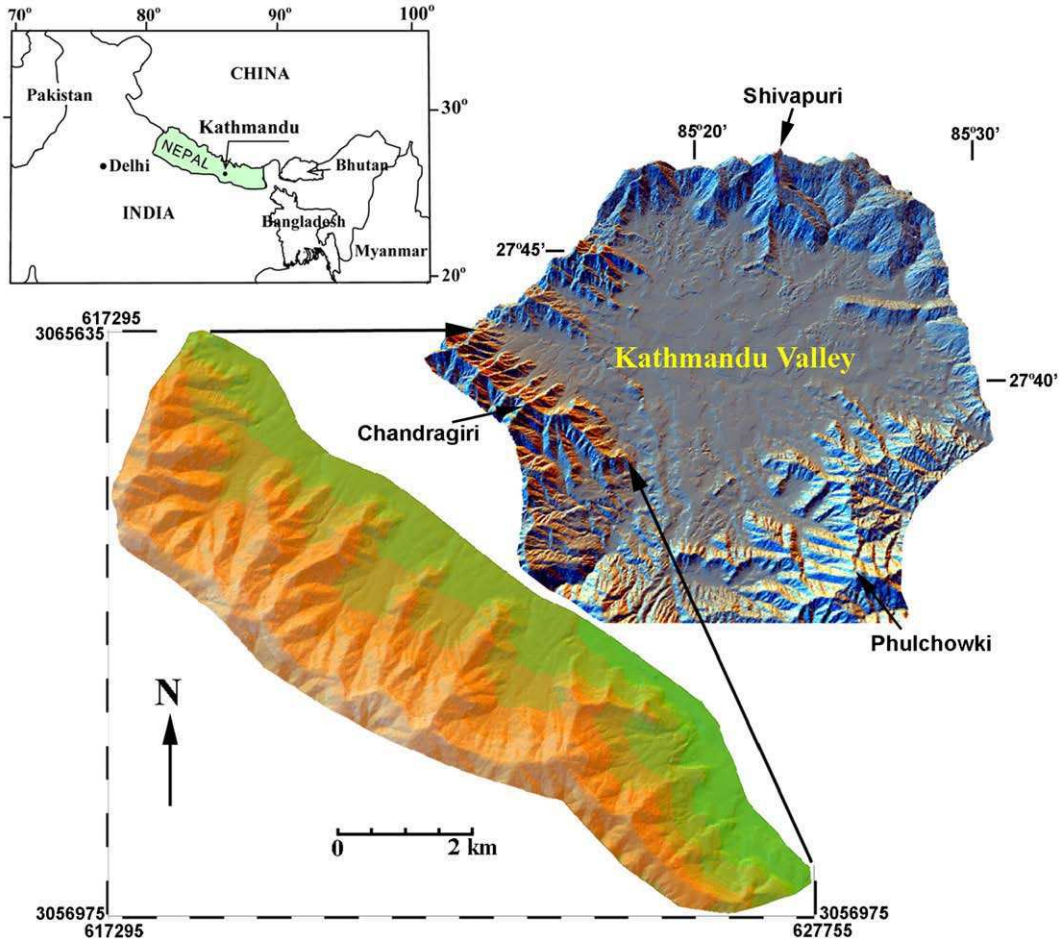

Fig. 1. Location maps of the study area. Coordinate values are from the Universal Transverse Mercator (UTM) projection system.

Please cite this article as: Dahal, R.K., et al., Predictive modelling of rainfall-induced landslide hazard in the Lesser Himalaya of Nepal based on weights-of-evidence, Geomorphology (2008), doi:10.1016/j.geomorph.2008.05.041

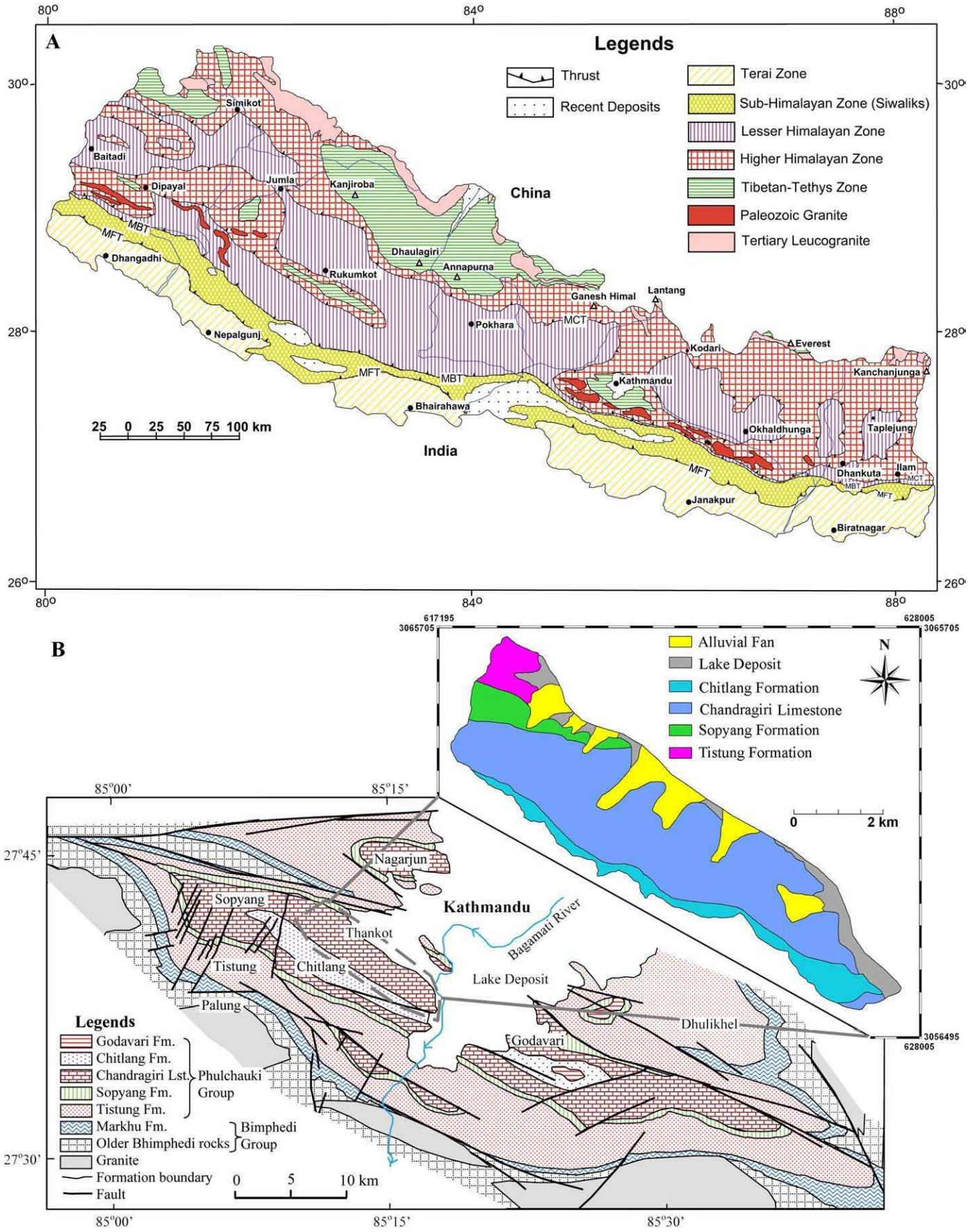

Fig. 2. Geological maps of A) Nepal (modified after Amatya and Jnawali, 1994, and Dahal, 2006) and B) South Kathmandu Valley (modified after Stöcklin and Bhattarai, 1977) with a geological map of the study area in the inset.

Please cite this article as: Dahal, R.K., et al., Predictive modelling of rainfall-induced landslide hazard in the Lesser Himalaya of Nepal based on weights-of-evidence, Geomorphology (2008), doi:10.1016/j.geomorph.2008.05.041

zones are most prone to landslides in the monsoon period. The study area is within the Lesser Himalaya and belongs to the Phulchauki and the Bhimphedi geologic groups, which together form the Kathmandu Complex (Stöcklin, 1980). The Bhimphedi Group consists of relatively high-grade metamorphic rocks of Precambrian age, whereas the Phulchauki Group is composed of weakly metamorphosed sediments of early to middle Palaeozoic age. The southern hills of the Kathmandu Valley consist of intensely folded and faulted metasediments, mainly limestone with a subordinate amount of shale and sandstone of the Phulchauki Group (Fig. 2B).

The study area ranges from 1400 to 2560 m in elevation with an area of 18.9 km^2. The mean annual precipitation ranges from 1500 to 2200 mm. Most slopes face north, and the slope gradient generally increases with increasing elevation. Colluvium is the main slope material above the bedrock. The area is mainly covered with a dense forest of immature trees and thorny shrubs. In 2002, the study area experienced extreme events of monsoon rainfall and faced huge losses of life and property. On July 23, 2002, monsoon storms dropped 300.1 mm of rain in a 24-h period. This is the highest precipitation in the area in the last 36 years. These rainfall events triggered 73 debris slides in the study area. Debris flows also occurred after the sliding. A single landslide occurred near the central part of the study area, killing 16 people (Dahal et al., 2006). According to the disaster history of the area and interviews with local residents, the 2002 disaster was the one of the worst natural disasters of that area in the last 50 years.

The area is on the outskirts of Kathmandu Metropolitan City in Nepal, and settlement at the base of the hills has risen sharply over the last 10 years. Because of the panoramic view of the Himalayas to the north, many residential areas have been developed without any consideration of landslide hazards. Some research has been conducted regarding landslide risk in the study area. Paudel et al. (2003) described a disaster management scenario for the central part of the study area, giving examples of the disastrous landslides of 2002. Paudyal and Dhital (2005) performed a statistical risk analysis for the southern part of Kathmandu, including the study area, and categorized the levels of risk as low, moderate and high. Dahal et al. (2006) provided a comprehensive description of the study area with respect to rainfall and landslides.

3. Weights-of-evidence modelling

In this study, weights-of-evidence modelling was used for the landslide hazard mapping. The method uses the Bayesian probability model, and was originally developed for mineral potential assessment (Bonham-Carter et al., 1988, 1989; Agterberg, 1992; Agterberg et al., 1993; Bonham-Carter, 2002). Several authors have applied the method to mineral potential mapping using GIS (Emmanuel et al., 2000; Harris et al., 2000; Tangestani and Moore, 2001; Carranza and Hale, 2002). Cheng (2004) also used the method to predict the location of flowing wells; Daneshfar and Benn (2002) used it to analyse spatial associations between faults and seismicity; and Zahiri et al. (2006) used it for mapping cliff instabilities associated with mine subsidence. The method has also been applied to landslide susceptibility mapping (Lee et al., 2002; Van Westen et al., 2003, Lee and Choi, 2004; Lee and Sambath, 2006; Dahal et al., 2008; Sharma and Kumar, 2008; Neuhäuser and Terhorst, 2007).

A detailed description of the mathematical formulation of the method is available in Bonham-Carter (2002). For landslide susceptibility modelling, the method calculates the weight for each landslide causative factor based on the presence or absence of the landslides within the area. Therefore, historical landslide data are essential for weighting factors. The modelling procedure also relies on the fundamental assumption that future landslides will occur under conditions similar to those contributing to past landslides. It also assumes that causative factors for the mapped landslides remain constant over time. The related mathematical relationships are described below.

Favourability of an incidence of landslide given the presence of the causative factor can be expressed by conditional probability (Bonham-Carter, 2002) as follows:

$$P\{L|F\} = \frac{P\{L \cap F\}}{P\{F\}} \tag{1}$$

where $P(L/F)$ is the conditional probability of the presence of a landslide (L) given the presence of a causative factor, F. Because $P\{L \cap F\}$ is equal to the proportion of the total area occupied by L and F together:

$$P\{L \cap F\} = \frac{N\{L \cap F\}}{N\{A\}} \tag{2}$$

and prior probability of landslide occurrence can be expressed by

$$P\{F\} = \frac{N\{F\}}{N\{A\}} \tag{3}$$

where $P\{F\}$ and $N\{F\}$ are the probability and area of causative factor, respectively. Similarly, $N\{A\}$is the total area of the region (Fig. 3). Substituting Eqs. (2) and (3) into Eq. (1) gives:

$$P\{L|F\} = \frac{N\{L \cap F\}}{N\{F\}} \tag{4}$$

In order to obtain an expression relating the posterior probability of L in terms of the prior probability to a multiplication factor, the conditional probability of being on F, given the presence of landslide, is defined as follows:

$$P\{F|L\} = \frac{P\{F|L\}}{P\{L\}} \tag{5}$$

Because $P\{F \cap L\}$ is the same as $P\{L \cap F\}$, Eqs. (1) and (5) can be combined to get $P\{L/F\}$, satisfying the relationship as follows:

$$P\{L|F\} = P\{L\}\frac{P\{F|L\}}{P\{F\}} \tag{6}$$

Eq. (6) reveals that the conditional or posterior probability of the landslide, given the presence of the causative factor, is equal to the prior probability of the landslide $P\{L\}$ multiplied by the factor $P\{F \cap L\}/P\{F\}$. A similar expression can be derived for the posterior probability of landslide occurring given the absence of the causative factor as follows:

$$P\{L|\overline{F}\} = P\{L\}\frac{P\{\overline{F}|L\}}{P\{\overline{F}\}} \tag{7}$$

where $\overline{L}$ is the absence of landslide and $\overline{F}$ is the absence of the landslide causative factor.

The probability model described here can be also expressed in odds form (Bonham-Carter, 2002). Weights-of-evidence modelling uses the natural logarithm of odds known as log odds or *Logits*. To convert Eq. (6) to odds, both sides are divided by $P\{\overline{L}\ |F\}$, leading to:

$$\frac{P\{L|F\}}{P\{\overline{L}|F\}} = \frac{P\{L\}P\{F|L\}}{P\{\overline{L}|F\}P\{F\}} \tag{8}$$

From the definitions of conditional probability:

$$P\{\overline{L}|F\} = \frac{P\{\overline{L} \cap F\}}{P\{F\}} = \frac{P\{F|\overline{L}\}P\{\overline{L}\}}{P\{F\}} \tag{9}$$

Rearranging Eqs. (8) and (9) gives the following equation:

$$\frac{P\{L|F\}}{P\{\overline{L}|F\}} = \frac{P\{L\}}{P\{\overline{L}\}}\frac{P\{F\}}{P\{F\}}\frac{P\{F|L\}}{P\{F|\overline{L}\}} \tag{10}$$

Please cite this article as: Dahal, R.K., et al., Predictive modelling of rainfall-induced landslide hazard in the Lesser Himalaya of Nepal based on weights-of-evidence, Geomorphology (2008), doi:10.1016/j.geomorph.2008.05.041

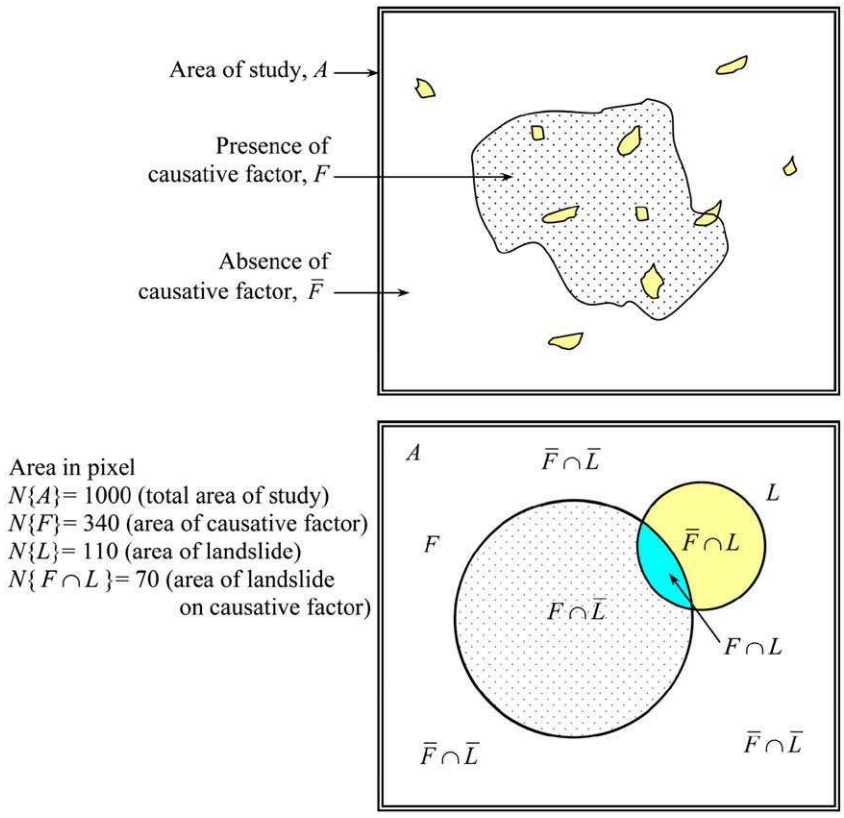

Fig. 3. Illustration of weights-of-evidence calculations (Modified after Bonham-Carter, 2002). The upper figure is an illustration of a causative factor map showing the location of landslides, and the lower figure is a Venn diagram summarizing the spatial overlap relationships between the causative factor and the landslides. Each landslide occupies a small unit area. The total area of study is shown as a rectangle (in the real field condition, it can be an irregularly shaped area). The areas of circles are not to scale.

Likewise, the odds of the presence of a landslide can be expressed as follows:

$$O\{L\} = \frac{P\{L\}}{1-P\{L\}} \tag{11}$$

and

$$O\{L\} = \frac{P\{L\}}{P\{\overline{L}\}} \tag{12}$$

Substituting Eq. (12) into Eq. (10) and cancelling of similar terms leads to:

$$O\{L|F\} = O\{L\}\frac{P\{F|L\}}{P\{F|\overline{L}\}} \tag{13}$$

where $O\{L/F\}$ is the conditional or posterior odds of a landslide given a causative factor. $O\{L\}$ is the prior odds of a landslide and $P\{F/L\}/P\{F/\overline{L}\}$ is known as the sufficient ratio (SR). In weights-of-evidence modelling, when the natural logarithms of both sides of Eq. (13) are taken, $\log_e SR$ gives positive weights of evidence, W_i^+(Bonham-Carter, 2002) and can be expressed as follows:

$$W_i^+ = \log_e \frac{P\{F|L\}}{P\{F|\overline{L}\}} \tag{14}$$

Similarly, for the case of odds, the following relation can be derived:

$$W_i^+ = \log_e \frac{O\{L|F\}}{O\{L\}} \tag{15}$$

Similar algebraic manipulation leads to the derivation of an odds expression for the conditional probability of landslides given the absence of the causative factor as follows:

$$O\{L|\overline{F}\} = O\{L\}\frac{P\{\overline{F}|L\}}{P\{\overline{F}|\overline{L}\}} \tag{16}$$

The term $P\{\overline{F}|L\}/P\{\overline{F}|\overline{L}\}$ is called the necessary ratio (NR). SR and NR are also known as likelihood ratios. In weights of evidence modelling, when the natural logarithms of both sides of Eq. (16) are taken, the $\log_e NR$ gives negative weights of evidence, W_i^-, as follows:

$$W_i^- = \log_e \frac{P\{\overline{F}|L\}}{P\{\overline{F}|\overline{L}\}} \tag{17}$$

Similarly, for the case of odds, the expression is as follows:

$$W_i^- = \log_e \frac{O\{L|\overline{F}\}}{O\{L\}} \tag{18}$$

In this research, the logarithm of likelihood ratios, i.e., Eqs. (14) and (17)), were used to calculate weights from the conditional probability value. A positive weight (W_i^+) indicates that the causative factor is present at the landslide location, and the magnitude of this weight is an indication of the positive correlation between presence of the causative factor and landslides. A negative weight (W_i^-) indicates an absence of the causative factor and shows the level of negative correlation. The difference between the two weights is known as the weight contrast, W_f ($=W_i^+ - W_i^-$), and the magnitude of contrast reflects the overall spatial association between the causative factor and landslides. In weights-of-evidence modelling, the combination of causative factors assumes that the

Please cite this article as: Dahal, R.K., et al., Predictive modelling of rainfall-induced landslide hazard in the Lesser Himalaya of Nepal based on weights-of-evidence, Geomorphology (2008), doi:10.1016/j.geomorph.2008.05.041

factors are conditionally independent of one another with respect to the landslides (Bonham-Carter, 2002; Lee and Choi, 2004). In this research, using bivariate statistics, the assumption is made that all landslides in a given study area occur under the same combination of parameters, and that all sets of parameters are conditionally independent.

Although weights-of-evidence modelling has not been previously applied in landslide hazard mapping of the Lesser Himalaya of Nepal, the suitability of the technique for this purpose is evident in its successful use in other studies for examining the distribution and spatial relationships of particular features. The area selected includes landslides triggered by rainfall, and the intrinsic variables are quantifiable in the field. Therefore, accurate landslide conditioning factor maps can be produced.

Debris slide and debris flow types of landslide (Varnes, 1984) have occurred predominantly in the study area. Only debris slide scars were considered in our study, because weights-of-evidence modelling can only be applied to single types of landslides. When different types of landslide are considered, the weights-of-evidence method needs to be applied separately to each type (Neuhäuser and Terhorst, 2007). All the debris flows in the study area were initiated after failure in topographic hollows in the upper reaches due to rainfall events, and thus our modelling deals with hazard associated with the areas prone to landslide initiation.

4. Data preparation

The main steps for landslide hazard mapping are data collection and the construction of a spatial database, from which relevant factors were extracted. This is followed by assessment of the landslide hazard using the relationship between landslides and causative factors, and the subsequent validation of results. A key feature of this method is that the possibility of landslide occurrence will be comparable with observed landslides.

For the hazard modelling, a number of thematic data of causative factors have been identified, including slope, slope aspect, geology, flow accumulation, relief, landuse, soil type, soil depth, distance to road, and mean annual rainfall. Topographic maps and aerial photographs provided by the Department of Survey, Government of Nepal were considered as basic data sources for generating these layers. Field surveys were carried out for data collection and to prepare data layers of various factors, as well as to prepare geological, soil-depth, soil-type and landuse maps. A landslide distribution map after the 2002 extreme monsoon rainfall events was also prepared in the field. These data sources were used to generate various thematic layers using the GIS software ILWIS 3.3. Brief descriptions of the preparation procedure of each data layer are provided here.

4.1. Landslide characteristics and inventory maps

A landslide inventory map is the simplest output of direct landslide mapping. It shows the location of discernible landslides. It is essential in landslide susceptibility mapping by weights-of-evidence modelling because the overlay analysis requires it.

Two types of landslide inventory maps for new and old landslides were prepared. For preparing the new-landslide map, landslides occurring after the 2002 extreme rainfall events were recorded in the field immediately after the events. As a consequence of the events, a total of 73 debris slide scars were detected in the study area.

For the old-landslide maps, 1:25,000 and 1:15,000 aerial photographs taken in 1979, 1989 and 1995 were used as a data source. Landslide scars were identified with stereoscopes, and the GIS data layer of the scars was prepared. For the 1:15,000 aerial photographs, epipolar stereo pairs were generated in ILWIS 3.3 and landslide inventory maps were also prepared from screen digitisations. Only landslide scars (main failure portions) were used to delineate the landslides. When preparing the landslide inventory maps from the photographs, especially the 1979 photos, only landslide scars having no vegetation were delineated. For the 1989 and 1995 photographs, the scars were cross-checked with the older photographs. The delineated landslide scars were also verified in the field. Although not all the old scars could be observed in the field because of vegetation, nearly 70% of the scars (especially those delineated from the 1989 and 1995 maps) were easily verified. New landslides were also observed within a few old landslide scars. A total of 119 landslide scars were delineated from the 1979, 1989, and 1995 photos. Rainfall data from the nearest rainfall station suggested that there were comparatively high monsoon rainfall events in 1978, 1979, 1987, 1988, and 1993. These events might be responsible for triggering the old landslides. The landslide inventory maps of both new and older landslides are shown in Fig. 4.

4.2. Geology

In this study, 11 factors (geology, slope, aspect, relief, distance to drainage flow accumulation, landuse, distance to road, soil depth, engineering soil type, and extreme one day rainfall) were selected as thematic data layers for analysis. Geology plays an important role in determining landslide susceptibility and hazard because different geological units have different susceptibilities to active geomorphological processes (Anbalagan, 1992; Pachauri et al., 1998; Dai et al., 2001). As mentioned in an earlier section, limestone, shale and metasandstone are the main rock types of the study area. For preparing the geological map, previous studies (Stöcklin and Bhattarai, 1977; Acharya, 2001) were consulted and geological boundaries of formations were checked and modified as per the field observations.

4.3. Topographic factors

A Digital Elevation Model (DEM) representing the terrain has been used to derive various geomorphological parameters which influence landslide activity. A DEM of the study area with 10×10 m cell size was prepared using digital contour data procured from the Department of Survey, Government of Nepal. From this DEM, geomorphological thematic data layers such as slope, aspect, relative relief, distance to drainage, and flow accumulation were prepared.

Slope, an important parameter in slope stability assessment, comprised seven classes (>5°, 5°–15°, 15°–25°, 25°–35°, 35°–45°, 45°–55° and >55°). This classification was determined after measuring slope angles of failed slope during landslide inventory mapping — most of the landslides occurred at slope angles between 25° and 55°. Aspect, the direction of maximum slope of the terrain surface, was divided into nine classes: N, NE, E, SE, S, SW, W, NW and Flat. Both slope and aspect were computed and mapped using available commands in ILWIS 3.3.

Relative relief is another DEM-based derivative, and is defined as the maximum height dispersion of a terrain normalized by its length or area (Oguchi, 1997). In this paper, relative relief is computed as the difference between the maximum and minimum altitudes within a given class of elevation. For this computation, elevation was sliced into twelve classes with 100 m bin, from 1400 to 2500 m.

In the study area, landslides occur frequently along streams due to groundwater movement towards stream and toe undercutting. Thus, distance of a landslide from a stream was considered as another geomorphology-related causative factor. To compute the distance, the drainage segment map was rasterised. A raster map was then constructed to show the distance with six classes: 0–10, 10–20, 20–30, 30–50, 50–100, and >100 m.

Following rainfall events, water flows from convex areas and accumulates in concave areas. This process is represented by the flow

Please cite this article as: Dahal, R.K., et al., Predictive modelling of rainfall-induced landslide hazard in the Lesser Himalaya of Nepal based on weights-of-evidence, Geomorphology (2008), doi:10.1016/j.geomorph.2008.05.041

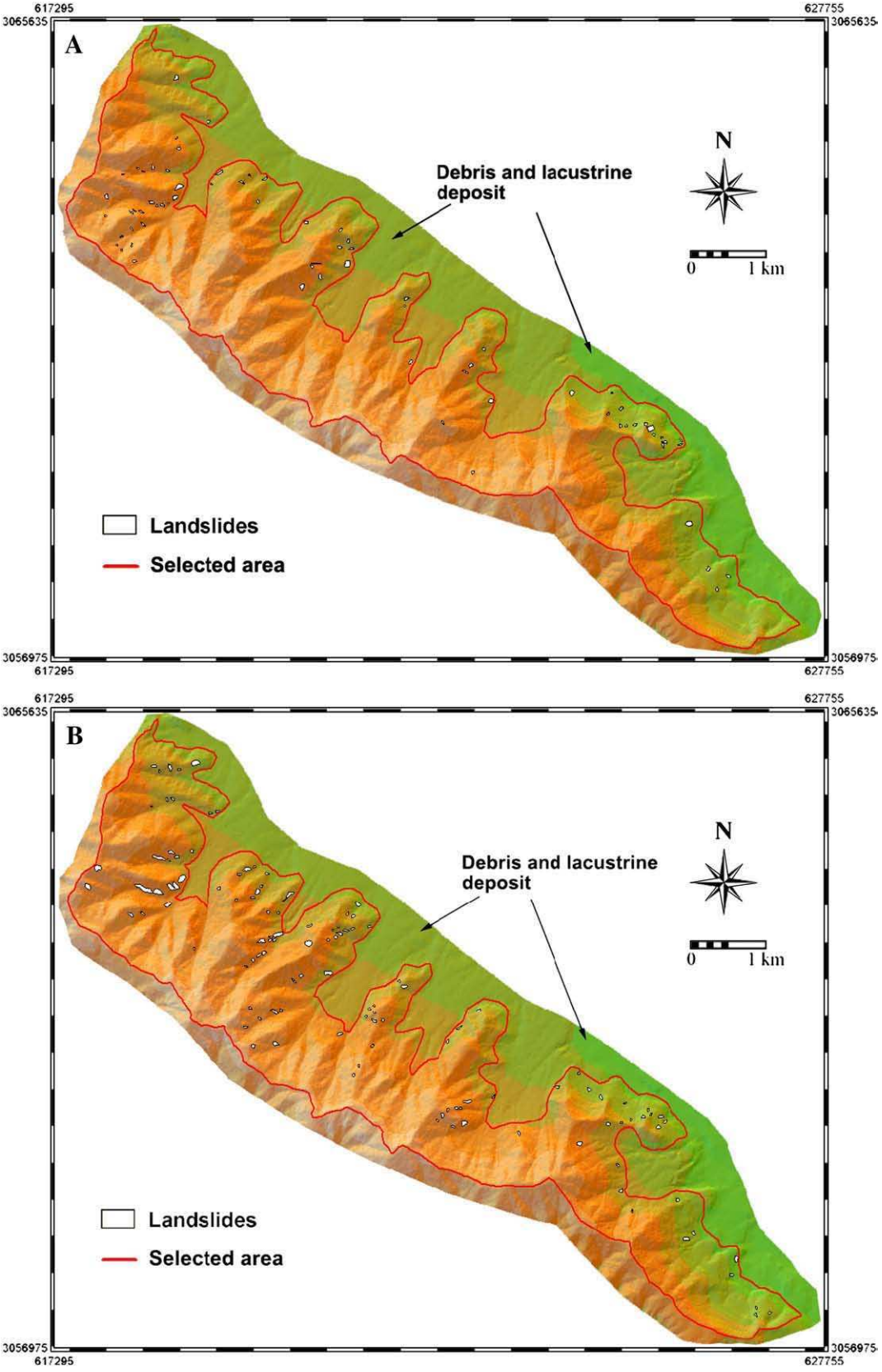

Fig. 4. Landslide inventory maps of the study area. A) Inventory map prepared after the 2002 extreme rainfall events. B) Inventory map prepared from aerial photographs of 1979, 1989, and 1995. The coordinate values are from the UTM projection system.

accumulation parameter, which is equivalent to the upstream area. This parameter was considered relevant to this study because it defines the locations of water concentration after rainfall and hence possible landslides. The flow accumulation map was prepared from the DEM using ILWIS 3.3, in which the parameter values were divided into eight classes based on histogram information.

Please cite this article as: Dahal, R.K., et al., Predictive modelling of rainfall-induced landslide hazard in the Lesser Himalaya of Nepal based on weights-of-evidence, Geomorphology (2008), doi:10.1016/j.geomorph.2008.05.041

4.4. Landuse

Landuse is also one of the key factors responsible for landslides. Vegetation prevents erosion through the natural anchorage provided by roots; thus, vegetated areas are less prone to landslides (Greenway, 1987; Styczen and Morgan, 1995). Based on field observations and mapping, six landuse classes that may have an impact on landslide activity were considered: dense forest, dry cultivated land, grassland, shrubs, sparse forest, and sparse shrub. The landuse was recorded in the field on a 1:25,000 topographical map. Subsequently the landuse data layer was generated as vector polygons and converted into a raster layer in GIS.

4.5. Distance to road

One of the controlling factors of slope stability is road construction. In the study area, many landslides occurred along roads and foot trails due to inappropriately cut slopes and drainage from the roads and trails. Thus, distance to road was calculated and mapped using the road and trail segment maps, and the obtained values were sliced into seven classes: 0–10, 10–20, 20–30, 30–50, 50–100, 100–200, and >200 m.

4.6. Soil depth and type

Soil mapping was performed for estimating soil depth and identifying engineering soil types. At first the study area was divided into 16 mosaics with more or less homogeneous topographic characteristics, on the basis of the pattern of contour lines and geomorphological setting (Fig. 5). Field observations suggested that soil thickness in each mosaic is usually homogeneous along a transverse section but varies along a longitudinal section. Thus, for each topographic mosaic, one to three longitudinal profiles were set and soil thickness was measured along them (Fig. 5). The measurement was made with a tape measure at outcrops along road cuts, trail cuts, gully erosion, old landslides and soil mines. Some outcrops were inaccessible because of thick forest around them and the absence of trails; in these cases, estimation was made from observations at nearby places. More measurements of soil depth were also made at other outcrops during field visits. More than 400 observation points were used in total, and a kriging interpolation with a rational quadratic semi-variogram was performed to interpolate the point values of soil depth into regularly distributed grid values. Before the interpolation, the spatial correlation of point data was investigated to obtain a semi-variogram with input parameters necessary for kriging (nugget, sill and range). The soil depth estimated from kriging was cross-checked in the field mainly for locations of rock exposure, and depths for rocky places were corrected as zero. Lastly, a soil-depth raster map was generated using the slicing method. The study of landslides after the 2002 extreme rainfall events suggested that soil depths of 0.5 to 2 m had maximum susceptibility to failure. There were also some failures in areas having 2 to 4 m soil depth. Thus, five soil depth classes were used: <1.0, 1–1.5, 1.5–2.5, 2.5–4.0, and >4 m.

A map of engineering soil types was also prepared from field observations, based on the procedure of NAVFAC (1986) and USBR (2001). Four main types of soil domains were identified: silty gravel, low plastic clay, silty sand and clayey to silty gravel. In accordance with the unified soil classification system (ASTM D 2487-83), the soil domains were named ML, CL, SM and GM to GC, respectively. Rocky terrains were independently classified as rock domain. The study area mainly consists of ML. SM and CL were recorded only in limited places. GM to GC was mainly found at the foot of hills such as old fan deposits.

4.7. Rainfall

Rainfall is an extrinsic variable in hazard analysis, and the spatial distribution of mean annual rainfall is often considered in statistical hazard analysis. However, the study area has many landslides

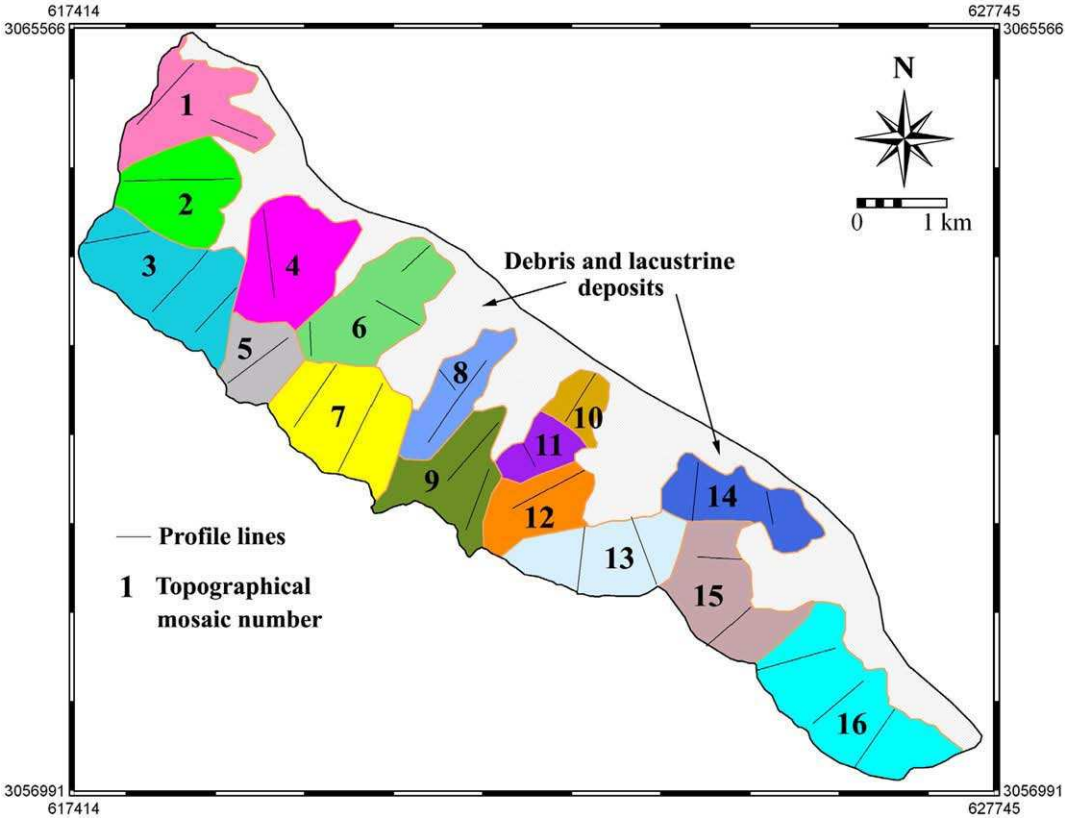

Fig. 5. Layout of 16 topographic mosaics and 29 profile lines used for soil thickness measurement. The coordinate values are from the UTM projection system.

Please cite this article as: Dahal, R.K., et al., Predictive modelling of rainfall-induced landslide hazard in the Lesser Himalaya of Nepal based on weights-of-evidence, Geomorphology (2008), doi:10.1016/j.geomorph.2008.05.041

Table 1
Computed weights for classes of various data layers based on the new landslides

Domain	Class	Landslide occurrences	% Occu.	No. of pixel in domain	% domain	Ratio % of occu./% of domain	Weight W^+	Weight W^-
1 Slope	<5°	0	0.000	1116	0.592	0.000	−1.865	0.005
	5 to 15°	23	2.122	7893	4.185	0.507	−0.682	0.021
	15 to 25°	154	14.207	30165	15.993	0.888	−0.119	0.021
	25 to 35°	460	42.435	63148	33.479	1.268	0.239	−0.145
	35 to 45°	239	22.048	43453	23.037	0.957	−0.044	0.013
	45 to 55°	125	11.531	28820	15.279	0.755	−0.283	0.044
	>55°	83	7.657	14024	7.435	1.030	0.030	−0.002
2 Aspect	Flat	13	1.199	5795	3.072	0.390	−0.944	0.019
	North	95	8.764	54942	29.129	0.301	−2.315	0.230
	North–East	258	23.801	53565	28.399	0.838	−0.178	0.063
	East	375	34.594	40429	21.434	1.614	0.482	−0.184
	South-East	223	20.572	23204	12.302	1.672	0.518	−0.100
	South	114	10.517	5775	3.062	3.435	1.248	−0.080
	South-West	5	0.461	779	0.413	1.117	0.111	0.000
	West	1	0.092	4130	2.190	0.042	−3.172	0.021
3 Flow accumulation	1 Cell	258	23.801	54223	28.747	0.828	−0.190	0.068
	3 Cells	221	20.387	38765	20.552	0.992	−0.008	0.002
	5 Cells	105	9.686	18033	9.561	1.013	0.013	−0.001
	10 Cells	135	12.454	22432	11.893	1.047	0.046	−0.006
	20 Cells	169	15.590	20053	10.631	1.466	0.386	−0.057
	50 Cells	118	10.886	19110	10.132	1.074	0.072	−0.008
	1000 Cells	76	7.011	14108	7.480	0.937	−0.065	0.005
	>1000 Cells	2	0.185	1895	1.005	0.184	−1.699	0.008
4 Relief	<1400 m	33	3.044	4264	2.261	1.347	0.300	−0.008
	1400–1500 m	133	12.269	10149	5.381	2.280	0.832	−0.076
	1500–1600 m	262	24.170	19314	10.240	2.360	0.867	−0.170
	1600–1700 m	197	18.173	26649	14.128	1.286	0.253	−0.049
	1700–1800 m	283	26.107	29473	15.626	1.671	0.517	−0.133
	1800–1900 m	64	5.904	26391	13.992	0.422	−0.866	0.090
	1900–2000 m	25	2.306	20454	10.844	0.213	−1.553	0.092
	2000–2100 m	60	5.535	17397	9.223	0.600	−0.513	0.040
	2100–2200 m	27	2.491	15212	8.065	0.309	−1.179	0.059
	2200–2300 m	0	0.000	11055	5.861	0.000	−4.158	0.060
	2300–2400 m	0	0.000	6448	3.419	0.000	−3.619	0.034
	>2300 m	0	0.000	1813	0.961	0.000	−2.350	0.009
5 Distance to drainages	0–10 m	64	5.904	20770	11.012	0.536	−0.626	0.056
	10–20 m	59	5.443	13654	7.239	0.752	−0.287	0.019
	20–30 m	81	7.472	15592	8.266	0.904	−0.102	0.009
	30–50 m	166	15.314	30517	16.179	0.947	−0.055	0.010
	50–100 m	335	30.904	55137	29.232	1.057	0.056	−0.024
	>100	379	34.963	52949	28.072	1.245	0.221	−0.101
6 Soil depth	<1.0 m	319	29.428	72259	38.310	0.768	−0.265	0.135
	1–1.5 m	357	32.934	65834	34.903	0.944	−0.058	0.030
	1.5–2.5 m	185	17.066	36788	19.504	0.875	−0.134	0.030
	2.5–4.0 m	198	18.266	11614	6.157	2.966	1.099	−0.139
	>4.0 m	25	2.306	2124	1.126	2.048	0.723	−0.012
7 Engineering soil type	CL	0	0.000	4293	2.276	0.000	−3.212	0.022
	GM and GC	254	23.432	33477	17.748	1.320	0.280	−0.072
	ML	732	67.528	137923	73.123	0.923	−0.080	0.190
	SM	3	0.277	7312	3.877	0.071	−2.645	0.037
	Rock	95	8.764	5614	2.976	2.944	1.091	−0.062
8 Geology	Alluvial Fan	19	1.753	2126	1.127	1.555	0.445	−0.006
	Lake Deposit	3	0.277	3184	1.688	0.164	−1.813	0.014
	Chitlang Formation	27	2.491	29398	15.586	0.160	−1.839	0.145
	Chandragiri Limestone	893	82.380	130998	69.451	1.186	0.172	−0.553
	Sopyang Formation	117	10.793	13552	7.185	1.502	0.410	−0.040
	Tistung Formation	25	2.306	9361	4.963	0.465	−0.769	0.028
9 Landuse	Dense Forest	427	39.391	146613	77.730	0.507	−0.683	1.011
	Dry Cultivated	227	20.941	14952	7.927	2.642	0.981	−0.153
	Grassland	0	0.000	1050	0.557	0.000	−1.804	0.005
	Shrubs	1	0.092	2072	1.099	0.084	−2.482	0.010
	Sparse Forest	237	21.863	19823	10.510	2.080	0.739	−0.136
	Sparse Shurb	192	17.712	4109	2.178	8.131	2.138	−0.174
10 Distance to roads	0–10 m	136	12.546	14198	7.527	1.667	0.515	−0.056
	10–20 m	93	8.579	8839	4.686	1.831	0.610	−0.042
	20–30 m	86	7.934	9472	5.022	1.580	0.461	−0.031
	30–50 m	102	9.410	14966	7.935	1.186	0.172	−0.016
	50–100 m	197	18.173	34141	18.101	1.004	0.004	−0.001
	100–200 m	222	20.480	45380	24.059	0.851	−0.162	0.046
	>200	248	22.878	61623	32.671	0.700	−0.358	0.137
11 Extreme one day rainfall	220–240 mm	406	37.454	69906	37.062	1.011	0.011	−0.006
	240–260 mm	44	4.059	36751	19.484	0.208	−1.573	0.176
	260–280 mm	487	44.926	66956	35.498	1.266	0.237	−0.159
	280–300 mm	147	13.561	15006	7.956	1.705	0.537	−0.063

Please cite this article as: Dahal, R.K., et al., Predictive modelling of rainfall-induced landslide hazard in the Lesser Himalaya of Nepal based on weights-of-evidence, Geomorphology (2008), doi:10.1016/j.geomorph.2008.05.041

triggered by extreme rainfall. Thus, extreme one-day rainfall records for 11 stations around the Kathmandu Valley were used to prepare a rainfall map. First, point values of extreme one-day rainfall were mapped, and the spatial distribution of rainfall was calculated through the application of the inverse distance squared method in ILWIS 3.3. The resulting map was sliced to give a raster map with four classes having a 20 mm interval: 220–240, 240–260, 260–280, and 280–300 mm.

5. Analysis and results

To evaluate the contribution of each factor to landslide hazard, both new and old landslide distribution data layers were compared separately with various thematic data layers. For this purpose, Eqs. (14) and (17) were rewritten according to numbers of cells as follows:

$$W_i^+ = \log_e \frac{\frac{Npix_1}{Npix_1+Npix_2}}{\frac{Npix_3}{Npix_3+Npix_4}} \quad (19)$$

$$W_i^- = \log_e \frac{\frac{Npix_2}{Npix_1+Npix_2}}{\frac{Npix_4}{Npix_3+Npix_4}} \quad (20)$$

where: $Npix_1$ is the number of cells representing the presence of both a potential landslide causative factor and landslides; $Npix_2$ is that representing the presence of landslides and absence of a potential landslide causative factor; $Npix_3$ is that representing the presence of a potential landslide causative factor and absence of landslides; and $Npix_4$ is that representing the absence of both a potential landslide causative factor and landslides.

All thematic maps were stored in raster format with a cell size of 10×10 m and were combined with one of the three landslide inventory maps (new, old and all landslides) for the calculation of W_i^+ and W_i^-. The calculation procedure was written in a script file of ILWIS 3.3, consisting of a series of GIS commands to support the use of Eqs. (19) and (20). All of the maps contain several classes, and the presence of one factor, such as silty soil, implies the absence of the other factors of the same soil type map. Therefore, in order to obtain the final weight of each factor, the positive weight of the factor itself was added to the negative weight of the other factors (Van Westen et al., 2003). The final calculated weights for new landslides are given in Table 1.

The resulting total weights, as shown in Table 1, directly indicate the importance of each factor. If the total weight is positive, the factor is favourable for the occurrence of landslides, whereas if it is negative, it is unfavourable. Some of the factors show little relation to the occurrence of landslides, as evidenced by weights close to zero. For example, some classes of flow accumulation, when crossed with all three maps, reveal values that oscillate around zero without any extreme positive or negative values, indicating that flow accumulation is less important. However, it does not mean that the role of flow accumulation must be exempted absolutely in the modelling, because its class domain has some weights. The frequency ratio (%landslide / %area) helps to assess the relationship between the factors and landslide occurrences (Lee and Sambath, 2006; Dahal et al., 2008). For example, slope aspects S, SE and SW show high probabilities of landslide occurrences, whereas north-facing slopes are less vulnerable. Field investigations of the orientation of rock joints indicate that slopes having S, SE and SW aspects were mainly dip slopes and had seepage problems, accounting for the high probability of landslide occurrences in S, SE and SW slopes.

The weights were assigned to the classes of each thematic layer, and the resultant weighted thematic maps were overlaid and numerically added to produce a Landslide Hazard Index (LHI) map:

$$\begin{aligned} LHI = {} & W_f\text{Slope} + W_f\text{Aspcls} + W_f\text{FA} + W_f\text{Relief} + W_f\text{Disdrn} \\ & + W_f\text{Depth} + W_f\text{Egsoil} + W_f\text{Geo} + W_f\text{Landuse} + W_f\text{Disrd} \\ & + W_f\text{Rnfall} \end{aligned} \quad (5)$$

where W_fSlope, W_fAspcls, W_fFA, W_fRelief, W_fDisdrn, W_fDepth, W_fEgsoil, W_fGeo, W_fLanduse, W_fDisrd, and W_fRnfall are distribution-derived weights of slope, slope aspect, flow accumulation, relief, distance to drainages, engineering soil type, geology, landuse, distance to roads, and extreme one day rainfall, respectively. Three attribute maps of different landslide cases were prepared from respective LHI values (Fig. 6), which were in the range from −15.662 to 8.231 for the new landslides, −12.483 to 6.769 for the old landslides, and −13.023 to 6.926 for all landslides. The ability of LHI to predict landslide occurrences was verified using the success rate curve (Chung and Fabbri, 1999), prediction rate, and effect analysis (Van Westen et al., 2003; Lee, 2004; Dahal et al., 2008). The success rate indicates what percentage of all landslides occurs in the classes with the highest value of susceptibility. When old landslides are used for LHI calculation and new landslides are used for prediction, the calculated accuracy rate is called prediction rate (Van Westen et al., 2003; Lee et al., 2007), and is the most suitable parameter for independent validation of LHI. Effect analysis helps to validate and to check the predictive power of selected factors that are used in hazard analysis.

5.1. Success rates

The success rate curves of all three maps are shown in Fig. 7. These curves are measures of goodness of fit. To obtain the success rate curve for each LHI map, the calculated index values of all cells in the maps were sorted in descending order. Then the ordered cell values were categorised into 100 classes with 1% cumulative intervals, and classified LHI maps were prepared with the slicing operation in ILWIS 3.3. These maps were crossed with the landslide inventory map. Then the success rate curve was created from the cross table values.

In the case of new landslides, the success rate reveals that 10% of the study area where LHI had a higher rank could explain 50% of total new landslides. Likewise, 30% of higher LHI value could explain 88% of all landslides. Similarly, for the cases of old landslides and all landslides, 30% high LHI value could explain about 80% of total landslides. Fig. 7 provides percentage coverage of landslides in various higher rank percentage of LHI. To compare the landslide hazard results, area under the curves (Lee, 2004; Dahal et al., 2008), a quantitative measure of the success rate of LHI, was estimated from the success rate graphs (Fig. 7). A total area equal to one denotes perfect prediction accuracy; whereas an area less than 0.5 shows that the model is invalid. In this study, area under the curves ranged from 0.8213 to 0.8595, meaning that the success rate ranged from 82% to 86% and thus the model is valid. Analysis of the new landslide case shows a higher value of success rate than the other two cases.

5.2. Effect analysis

The three LHI maps (Fig. 6) were prepared by referencing the eleven factor maps. In the weights-of-evidence modelling, the effect of factor maps is very critical (Lee and Choi, 2004) and effect analysis suggests the predictive power of factor maps. The modelling assumes that the factors are conditionally independent of one another with respect to the landslides (Van Westen et al., 2003; Zahiri et al., 2006; Dahal et al.; 2008, Sharma and Kumar, 2008), which is a precondition for the modelling (Lee et al., 2002; Lee and Choi, 2004; Neuhäuser and Terhorst, 2007). We also tested the conditional independency of factors to acquire a high success rate. The pair-wise test suggests that out of the 10 intrinsic variables, aspect, flow accumulation, distance to drainage and soil depth reveal conditional independence with Chi-square values less than 2.8. The existing research also suggests that utilization of geomorphology-related parameters in hazard evaluation is very promising (Van Westen et al., 2003), and parameters related to geomorphology, geology and human intervention are considered most effective for hazard evaluation. Thus, the following five combinations were selected for the effect analysis.

Please cite this article as: Dahal, R.K., et al., Predictive modelling of rainfall-induced landslide hazard in the Lesser Himalaya of Nepal based on weights-of-evidence, Geomorphology (2008), doi:10.1016/j.geomorph.2008.05.041

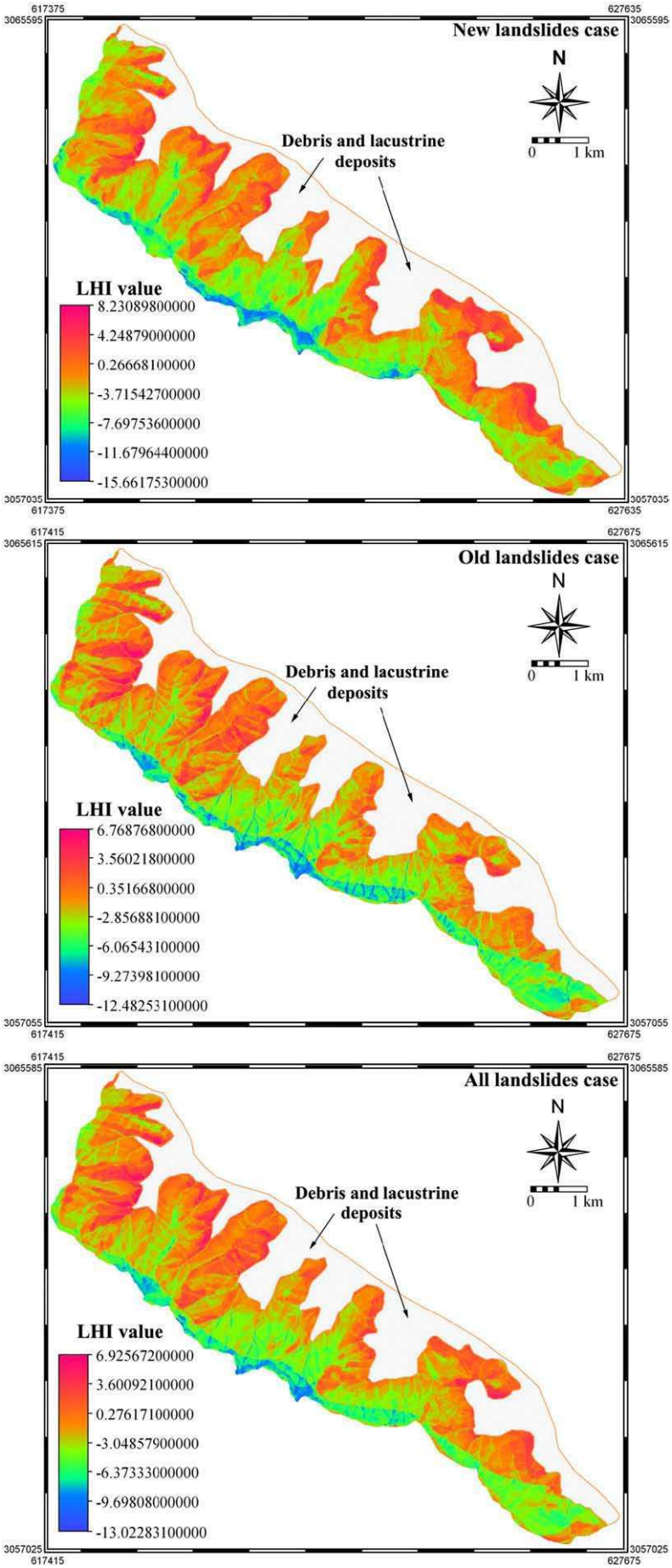

Fig. 6. LHI maps of the new, old and all landslides cases. The coordinate values are from the UTM projection system.

Please cite this article as: Dahal, R.K., et al., Predictive modelling of rainfall-induced landslide hazard in the Lesser Himalaya of Nepal based on weights-of-evidence, Geomorphology (2008), doi:10.1016/j.geomorph.2008.05.041

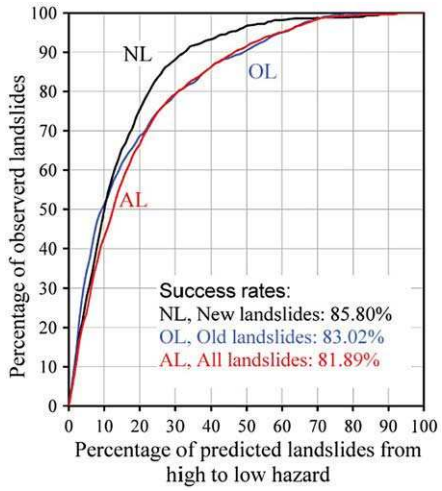

Fig. 7. Success rate curves of landslide hazard values calculated from the three types of landslide inventory maps. The areas under the curve for all three cases were determined by assuming a total area of 100 (X)× 100 (Y) units. Other details are in text.

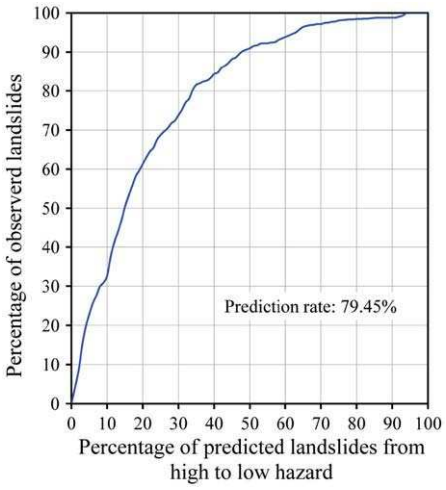

Fig. 8. Prediction rate curves of landslide hazard values calculated from the inventory map of the old landslides.

Comb-1: Only geomorphology-related factor maps (W_fSlope, W_fAspcls, W_fFA, W_fRelief, W_fDisdrn, and W_fRnfall).
Comb-2: Geomorphology and geology-related factors maps (W_fSlope, W_fAspcls, W_fFA, W_fRelief, W_fDisdrn, W_fDepth, W_fEgsoil, W_fGeo, and W_fRnfall).
Comb-3: Geomorphology and human intervention-related factor maps (W_fSlope, W_fAspcls, W_fFA, W_fRelief, W_fDisdrn, W_fLanduse, W_fDisrd, and W_fRnfall)
Comb-4: Geology and human intervention-related factor maps (W_fDepth, W_fEgsoil, W_fGeo, W_fLanduse, W_fDisrd, and W_fRnfall)
Comb-5: Factor maps showing conditional independence (W_fAspcls, W_fFA, W_fDepth, W_fDisdrn, and W_fRnfall)

Being an extrinsic variable, the rainfall factor was used in all combinations.

To compare the landslide hazard value of all five combinations along with all the factors map (calculated as per Eq. (5)); both success and prediction rates were calculated from the area under the curve of the rate graphs. Four cases of landslide maps were considered: Case I — LHI of new landslides crossed with same landslide map; Case II — LHI of old landslides crossed with same landslide map; Case III — LHI of all landslides crossed with same landslide map; and Case IV — LHI of old landslides crossed with new landslide map. Cases I, II, and III suggest success rates similar to the resulting LHI values. The validation of LHI values from the success rate is common in previous studies of this kind due to a lack of time-based landslide data. In this study, however, both old and new landslide inventory maps were available and independent validation of LHI value was possible through the calculation of a prediction rate. Thus, Case IV was the most informative validation procedure.

Table 2 shows that the success rates of this modelling procedure varied from 66% to 86%. Case I with all factor map combinations shows the maximum success rates. Cases I, II and III have lower success rates in Comb-5, implying that modelling only with conditional independent factors may not be effective. By contrast, geomorphology and human intervention-related factor maps (Comb-3) show high success rates.

The prediction rate in Case IV is similar to the success rates of Cases I, II and III with various combinations of maps. Case IV is independent, and when all maps were combined for the LHI calculation, it gave 79.45% prediction accuracy for the old landslides (Fig. 8). More than 74% of the new landslides were well covered by 30% of the high value of LHI calculated from the old landslides. Fig. 9 demonstrates predicted landslide percentages in 10%, 50% and 70% of high value LHI for various combinations of factor maps. Comb-2, Comb-3 and the all maps combinations showed better coverage of predicted landslides at 30% of the high value of landslide hazard.

5.3. Classified hazard maps

For providing classified hazard maps, reference to prediction rate curves (see Fig. 8) was made and five landslide hazard classes were defined: very low (<30% class of low to high LHI values), low (30–50% class of low to high LHI values), moderate (50–70% class of low to high LHI values), high (70–90% class of low to high LHI values), and very high (>90% class of low to high LHI values) were established. Then, two classified hazard maps were prepared for the new landslides (Map 1) and the old landslides (Map 2).

Although Map 1 showed a high success rate, it is not the best hazard map for the study area because its prediction rate could not be estimated. Map 2 also could not be used as the final hazard map, although its prediction rate could be determined because Map 1 consisted of a considerable amount of high hazard value cells with respect to Map 2. Therefore, to consider the distribution of higher

Table 2
Area under the curve and success rate for all cases and combinations, after weights-of-evidence modelling

Cases		Scenarios	All maps	Comb-1	Comb-2	Comb-3	Comb-4	Comb-5
I	LHI value of new landslides crossed with same landslide map	Ratio of the area under the curve	0.858	0.800	0.833	0.840	0.800	0.749
		Success rate (%)	85.802	79.994	83.254	83.974	80.015	74.884
II	LHI value of old landslides crossed with same landslide map	Ratio of the area under the curve	0.830	0.788	0.810	0.812	0.694	0.765
		Success rate (%)	83.030	78.778	81.024	81.206	0.694	76.542
III	LHI value of all	Ratio of the area under the curve	0.819	0.774	0.798	0.804	0.729	0.746
	Landslides crossed with same landslide map	Success rate (%)	81.889	77.370	79.794	80.382	72.936	74.570
IV	LHI value of old	Ratio of the area under the curve	0.795	0.704	0.744	0.767	0.664	0.677
	Landslides crossed with new landslide map	Prediction rate (%)	79.454	70.401	74.357	76.745	66.411	67.668

Details are in text.

Please cite this article as: Dahal, R.K., et al., Predictive modelling of rainfall-induced landslide hazard in the Lesser Himalaya of Nepal based on weights-of-evidence, Geomorphology (2008), doi:10.1016/j.geomorph.2008.05.041

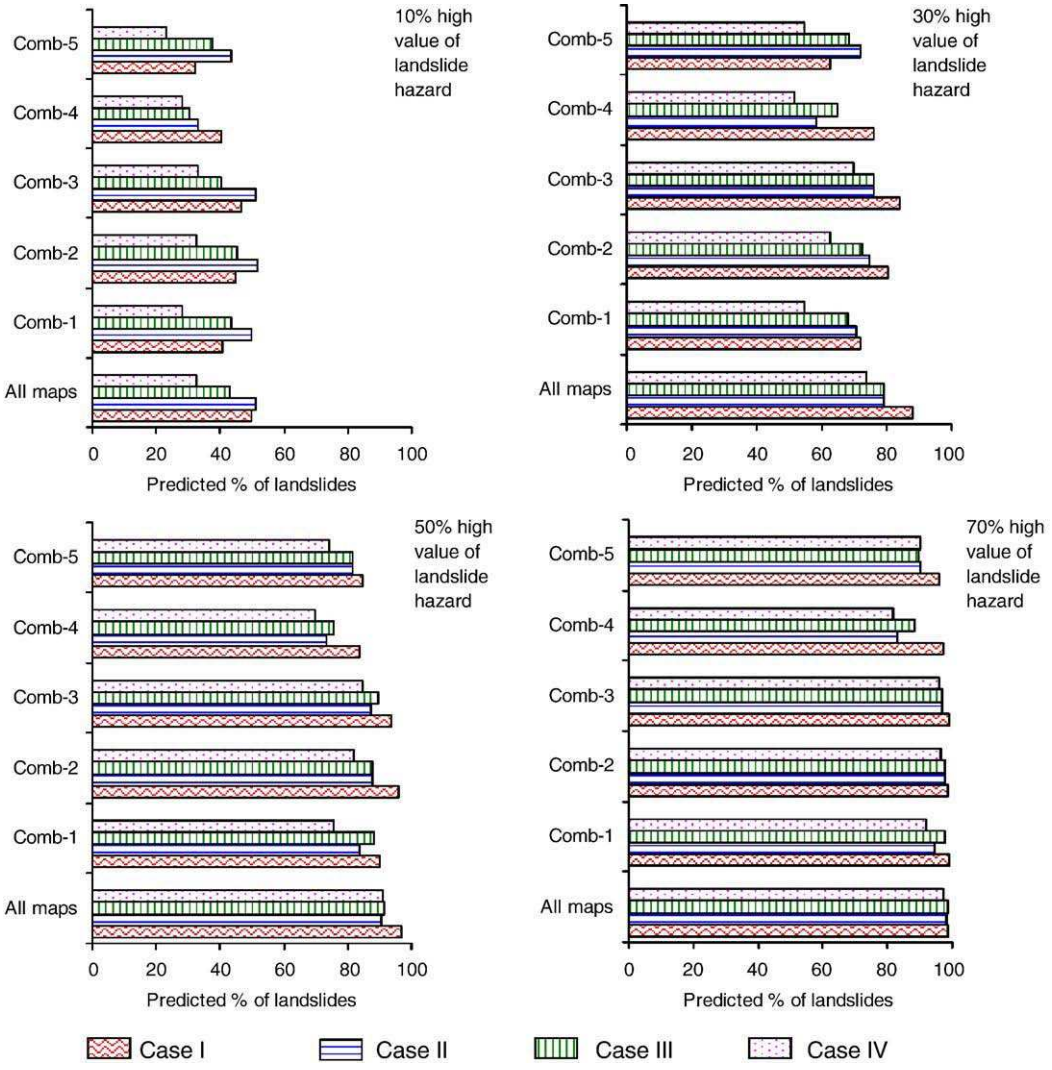

Fig. 9. Landslide prediction scenarios based on high landslide hazard value. Comb-1 represents geomorphology-related factors. Comb-2 — geomorphology and geology-related factors. Comb-3 — geomorphology and human intervention-related factors. Comb-4 — geology and human intervention-related factors. Comb-5 — factors showing conditional independence. Case I corresponds to LHI of the new landslides crossed with the same landslide map; Case II — LHI of the old landslides crossed with the same landslide map; Case III — LHI of all landslides crossed with the same landslide map; and Case IV — LHI of the old landslides crossed with the new landslide map.

value hazard cells in both maps, Map 1 was modified using some landslide hazard values of Map 2. For this purpose, cells of very high hazard, high hazard, moderate hazard and low hazard classes of Map 2 were transferred to Map 1 using commands and operations in ILWIS 3.3. In this process, a large number of cells having very low hazard, low hazard and moderate hazard classes in Map 1 were changed to a high hazard class. The resulting hazard map was again compared with the new landslides, giving a very high goodness of fit (88.4%; Fig. 10). Similarly, in this hazard map, if 20% of the classes have high landslide hazard value for future landslides, 81% of the landslides can be correctly fit. The final landslide hazard classification map for the study area is shown in Fig. 11. This map and Table 3 show the relation between the distribution of the old and new landslides and the classified hazard map, and the results seem to be reasonable. For example, the Very High Hazard (VHH) and High Hazard (HH) classes correspond to 86.0% of the old landslides and 91.1% of the new landslides, respectively.

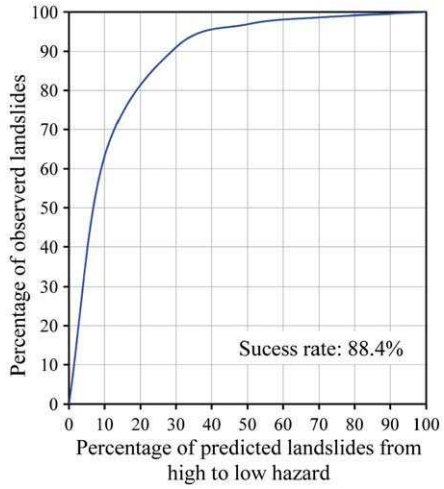

Fig. 10. Success rate curve of the final landslide hazard map.

6. Conclusions

Landslide hazard mapping is essential in delineating landslide prone areas in mountainous regions. Various methodologies have been proposed for landslide susceptibility and hazard mapping. This study applied weights-of-evidence modelling with bivariate statistical methods to the south-western hills of Kathmandu, in the Lesser Himalaya of Nepal, considering 10 intrinsic factors and one extrinsic

Please cite this article as: Dahal, R.K., et al., Predictive modelling of rainfall-induced landslide hazard in the Lesser Himalaya of Nepal based on weights-of-evidence, Geomorphology (2008), doi:10.1016/j.geomorph.2008.05.041

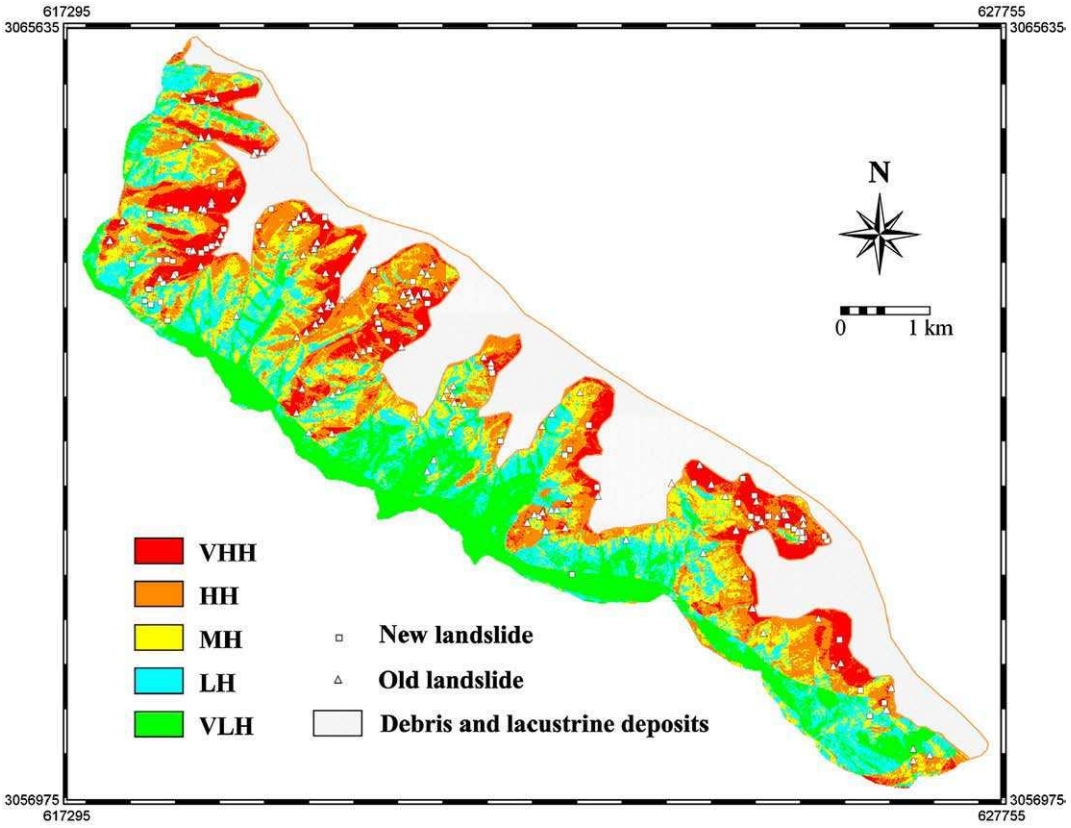

Fig. 11. Final classified landslide hazard map of the south-western hills of the Kathmandu Valley after weights-of-evidence modelling. VHH: very high hazard, HH: high hazard, MH: moderate hazard, LH: low hazard, VLH: very low hazard. The coordinate values are from the UTM projection system.

factor affecting landslides. The thematic layers of all causative factors and existing landslides were prepared in GIS (ILWIS 3.3), based mainly on DEM-based topographic parameters, existing maps and field data. The conclusions can be summarized as follows:

- The landslide hazard values estimated from landslide data for different periods and eleven factor maps have more or less similar degrees of accuracy ranging from 80% to 86%.
- In many approaches to weights-of-evidence modelling of landslide hazard or susceptibility in GIS, the model validation process tends to be dependent on the trained landslide data and the same landslide data are often used for verification. In contrast, this study verified the model independently using time-based new landslide data, giving a prediction rate of 80%. This validates the effectiveness of this modelling.
- The final landslide hazard map, prepared after the combination of hazard values for the older and new landslides, was found to be most acceptable for the study area with a success rate of 88.4%.
- The evaluation of predictive factors used in our modelling suggests that the roles of geomorphology and human intervention are very significant for landslide processes in the Lesser Himalaya of Nepal.

Table 3
Distribution ratios of the old and new landslides in the classified hazard map after weights-of-evidence modeling

Hazard classes	Old landslides (%)	New landslides (%)
Very High Hazard (VHH)	59.3	63.1
High Hazard (HH)	26.7	28.0
Moderate Hazard (MH)	8.6	5.9
Low Hazard (LH)	4.8	1.8
Very Low Hazard (VLH)	0.6	1.3

- The probability values from this kind of predictive modelling are not absolute and represent only a relative degree of hazard. However, they can provide a measure of landslide initiation localities. Our methodology seems to have extensive applicability to the Lesser Himalaya of Nepal, with the limitation that knowledge of past landslide information affects the final probability values calculated by the model.

Acknowledgments

We thank Mr. Birendra Piya, a senior geologist, the Department of Mines and Geology, Government of Nepal, Kathmandu, for his technical assistance. We also acknowledge local community forest user groups of the study area for providing permission to enter the forest for investigation. Mr. Anjan Kumar Dahal and Ms. Seiko Tsuruta are sincerely acknowledged for their technical support during the preparation of this paper. The authors are grateful for the detailed review comments from Takashi Oguchi, Jan Kalvoda and two anonymous reviewers. The study has been partly funded by the Sasakawa Fund for Scientific Research, The Japan Science Society.

References

Acharya, K.K., 2001. Geology and structure of the Pharping — Raniban area central Nepal, M. Sc. Thesis, Central Department of Geology, Tribhuvan University, Nepal (Unpublished, 58 pp).

Agterberg, F.P., 1992. Combining indicator patterns in weights of evidence modeling for resource evaluation. Natural Resources Research 1 (1), 39–50.

Agterberg, F.P., Bonham-Carter, G.F., Cheng, Q., Wright, D.F., 1993. Weights of evidence modeling and weighted logistic regression for mineral potential mapping. In: Davis, J.C., Herzfeld, U.C. (Eds.), Computers in Geology, 25 Years of Progress. Oxford University Press, Oxford, pp. 13–32.

Amatya, K.M., Jnawali, B.M., 1994. Geological map of Nepal. Scale: 1:1,000,000. Department of Mines and Geology, Kathmandu, Nepal.

Please cite this article as: Dahal, R.K., et al., Predictive modelling of rainfall-induced landslide hazard in the Lesser Himalaya of Nepal based on weights-of-evidence, Geomorphology (2008), doi:10.1016/j.geomorph.2008.05.041

Anbalagan, D., 1992. Landslide hazard evaluation and zonation mapping in mountainous terrain. Engineering Geology 32, 269–277.
ASTM D 2487-83, Standard classification of soils for engineering purposes (Unified Soil Classification System). ASTM International, 100 Bar, harbor Drive, west Conshohocken, PA 19428, USA.
Atkinson, P.M., Massari, R., 1998. Generalized linear modelling of landslide susceptibility in the Central Apennines, Italy. Computer Geoscience 24, 373–385.
Bonham-Carter, G.F., 2002. Geographic information systems for geoscientist: Modelling with GIS. In: Merriam, D.F. (Ed.), Computer Methods in the Geosciences, vol. 13. Pergamon/Elsevier, New York, pp. 302–334.
Bonham-Carter, G.F., Agterberg, F.P., Wright, D.F., 1988. Integration of geological datasets for gold exploration in Nova Scotia. Photogramatic Engineering and Remote Sensing 54, 1585–1592.
Bonham-Carter, G.F., Agterberg, F.P., Wright, D.F., 1989. Weights of evidence modelling: a new approach to mapping mineral potential. Statistical Applications in the Earth Science, Geological Survey of Canada Paper 89–9, 171–183.
Carranza, E.J.M., Hale, M., 2002. Spatial association of mineral occurrences and curvilinear geological features. Mathmatical Geology 34, 203–221.
Çevik, E., Topal, T., 2003. GIS-based landslide susceptibility mapping for a problematic segment of the natural gas pipeline, Hendek (Turkey). Environmental Geology 44, 949–962.
Cheng, Q., 2004. Application of weights of evidence method for assessment of flowing wells in the Greater Toronto area, Canada. Natural Resource Research 13, 77–86.
Chung, C.-J.F., Fabbri, A.G., 1999. Probabilistic prediction models for landslide hazard mapping. Photogrammetric Engineering and Remote Sensing 65, 1389–1399.
Chung, C.-J.F., Fabbri, A.G., 2003. Validation of spatial prediction models for landslide hazard mapping. Natural Hazards 30, 451–472.
Dahal, R.K., 2006. Geology for Technical Students — A textbook for Bachelor Level Students. Bhrikuti Academic Publication, Exhibition Road, Kathmandu, Nepal. 756 pp.
Dahal, R.K., Hasegawa, S., Yamanaka, M., Nishino, K., 2006. Rainfall triggered flow-like landslides: understanding from southern hills of Kathmandu, Nepal and northern Shikoku, Japan. Proc 10th Int Congr of IAEG, The Geological Society of London, IAEG2006 Paper number 819, 1–14 (CD-ROM).
Dahal, R.K., Hasegawa, S., Nonomura, A., Yamanaka, M., Masuda, T., Nishino, K., 2008. GIS-based weights-of-evidence modelling of rainfall-induced landslides in small catchments for landslide susceptibility mapping. Environmental Geology 54 (2), 314–324.
Dai, F.C., Lee, C.F., Li, J., Xu, Z.W., 2001. Assessment of landslide susceptibility on the natural terrain of Lantau Island, Hong Kong. Environmental Geology 40, 381–391.
Daneshfar, B., Benn, K., 2002. Spatial relationships between natural seismicity and faults, southeastern Ontario and north-central New York state. Tectonophysics 353, 31–44.
Emmanuel, J., Carranza, M., Hale, M., 2000. Geologically constrained probabilistic mapping of gold potential, Baguio district, Philippines. Natural Resource Research 9, 237–253.
Ganser, A., 1964. Geology of the Himalaya. Inter Science John Wiley, London. 289 pp.
Gökceoglu, C., Aksoy, H., 1996. Landslide susceptibility mapping of the slopes in the residual soils of the Mengen region (Turkey) by deterministic stability analyses and image processing techniques. Engineering Geology 44, 147–161.
Greenway, D.R., 1987. Vegetation and slope stability. In: Anderson, M.G., Richards, K.S. (Eds.), Slope Stability. Wiley, New York, pp. 187–230.
Guzetti, F., Carrara, A., Cardinali, M., Rei, chen bach, P., 1999. Landslide hazard evaluation: a review of current techniques and their application in a multi-scale study, central Italy. Geomorphology 31, 181–216.
Harris, J.R., Wilkinson, L., Grunsky, E.C., 2000. Effective use and interpretation of lithogeochemical data in regional mineral exploration programs: application of geographic information systems (GIS) technology. Ore Geology Reviews 16, 107–143.
Lee, S., 2004. Application of likelihood ratio and logistic regression models to landslide susceptibility mapping in GIS. Environmental Management 34, 223–232.
Lee, S., Min, K., 2001. Statistical analysis of landslide susceptibility at Yongin, Korea. Environmental Geology 40, 1095–1113.
Lee, S., Choi, J., 2004. Landslide susceptibility mapping using GIS and the weights-of-evidence model. International Journal of Geogrgaphical Information Science 18, 789–814.
Lee, S., Sambath, T., 2006. Landslide susceptibility mapping in the Damrei Romel area, Cambodia using frequency ratio and logistic regression models. Environmental Geology 50, 847–855.
Lee, S., Choi, J., Min, K., 2002. Landslide susceptibility analysis and verification using the Bayesian probability model. Environmental Geology 43, 120–131.
Lee, S., Ryu, J., Kim, I., 2007. Landslide susceptibility analysis and its verification using likelihood ratio, logistic regression and artificial neural network models: case study of Youngin, Korea. Landslides 4, 327–338.
NAVFAC, 1986. Design Manual: Soil Mechanics, Revised Edition. U.S. Dept of Defence, NAVFAC DM-7.01. Department of the Navy, 389 pp. Washington DC.
Neuhäuser, B., Terhorst, G., 2007. Landslide susceptibility assessment using "weights-of-evidence" applied to a study area at the Jurassic escarpment (SW-Germany). Geomorphology 86, 12–24.
Oguchi, T., 1997. Drainage density and relative relief in humid steep mountains with frequent slope failure. Earth Surface Processes and Landforms 22, 107–120.
Pachauri, A.K., Gupta, P.V., Chander, R., 1998. Landslide zoning in a part of the Garhwal Himalayas. Environmental Geology 36, 325–334.
Paudel, P.P., Omura, H., Kubota, T., Morita, K., 2003. Landslide damage and disaster management system in Nepal. Disaster Prevention and Management 12, 413–419.
Paudyal, P., Dhital, M.R., 2005. Landslide hazard and risk zonation of Thankot–Chalnakhel area, central Nepal. Journal of Nepal Geological Society 31, 43–50.
Remondo, J., González, A., Ramón, J., Cendrero, A., Fabbri, A., Chung, C.-J.F., 2003. Validation of landslide susceptibility maps: examples and applications from a case study in Northern Spain. Natural Hazards 30, 437–449.
Saha, A.K., Gupta, R.P., Sarkar, I., Arora, M.K., Csaplovics, E., 2005. An approach for GIS-based statistical landslide susceptibility zonation — with a case study in the Himalayas. Landslides 2, 61–69.
Sharma, M., Kumar, R., 2008. GIS-based landslide hazard zonation: a case study from the Parwanoo area, Lesser and Outer Himalaya, H.P., India. Bulletin of Engineering Geology and the Environment 67, 129–137.
Siddle, H.J., Jones, D.B., Payne, H.R., 1991. Development of a methodology for landslip potential mapping in the Rhondda Valley. In: Chandler, R.J. (Ed.), Slope Stability Engineering. Thomas Telford, London, pp. 137–142.
Stöcklin, J., 1980. Geology of Nepal and its regional frame. Journal of the Geological Society London 137, 1–34.
Stöcklin, J., Bhattarai, K.D., 1977. Geology of Kathmandu area and Central Mahabharat Range Nepal Himalaya Kathmandu. HMG/UNDP Mineral Exploration Project, Technical Report, New York. 64 pp.
Styczen, M.E., Morgan, R.P.C., 1995. Engineering properties of vegetation. In: Morgan, R.P.C., Rickson, R.J. (Eds.), Slope Stabilisation and Erosion Control: a Bioengineering Approach. E&FN Spon, London, pp. 5–58.
Süzen, M.L., Doyuran, V., 2004. A comparison of the GIS based landslide susceptibility assessment methods: multivariate versus bivariate. Environmental Geology 45, 665–679.
Tangestani, M.H., Moore, F., 2001. Porphyry copper potential mapping using the weights-of-evidence model in a GIS, northern Shahr-e-Babak, Iran. Australian Journal of Earth Science 48, 695–701.
Terlien, M.T.J., 1996. Modelling spatial and temporal variations in rainfall-triggered landslides, PhD thesis, ITC Publ. Nr. 32, Enschede, The Netherlands, 254 pp.
USBR, 2001. Engineering Geology Field Manual, Second Edition Vol. I. U.S. Department of the Interior Bureau of Reclamation. 432 pp.
Van Westen, C.J., 2000. The modelling of landslide hazards using GIS. Survey in Geophysics 21, 241–255.
Van Westen, C.J., Terlien, T.J., 1996. An approach towards deterministic landslide hazard analysis in GIS. A case study from Manizales (Colombia). Earth Surface Process and Landforms 21, 853–868.
Van Westen, C.J., Rengers, N., Soeters, R., 2003. Use of geomorphological information in indirect landslide susceptibility assessment. Natural Hazards 30, 399–419.
Varnes, D.J., 1984. Landslide hazard zonation: a review of principles and practice. Commission on landslides of the IAEG, UNESCO, Natural Hazards No. 3. 61 pp.
Wu, W., Sidle, R.C., 1995. A distributed slope stability model for steep forested basins. Water Resource Research 31, 2097–2110.
Yin, K.L., Yan, T.Z., 1988. Statistical prediction model for slope instability of metamorphosed rocks. Proceedings of 5th Int Symp on Landslides, Vol. 2, Lausanne, Switzerland, pp. 1269–1272.
Zahiri, H., Palamara, D.R., Flentje, P., Brassington, G.M., Baafi, E., 2006. A GIS-based weights-of-evidence model for mapping cliff instabilities associated with mine subsidence. Environmental Geology 51, 377–386.
Zêzere, J.L., Rodrigues, M.L., Reis, E., Garcia, R., Oliveira, S., Vieira, G., Ferreira, A.B., 2004. Spatial and temporal data management for the probabilitic landslide hazard assessment considering landslide typology. In: Lacerda, W.A., Ehrlich, M., Fontura, S.A.B., Sayão, A.S.F. (Eds.), Landslides: Evaluation and Stabilization, Vol. 1. Taylor & Fancis Group, London, pp. 117–123. V 1.

Please cite this article as: Dahal, R.K., et al., Predictive modelling of rainfall-induced landslide hazard in the Lesser Himalaya of Nepal based on weights-of-evidence, Geomorphology (2008), doi:10.1016/j.geomorph.2008.05.041